

Automatic Construction of Lane-level HD Maps for Urban Scenes

Yiyang Zhou^{*1} and Yuichi Takeda^{*2} and Masayoshi Tomizuka¹ and Wei Zhan¹

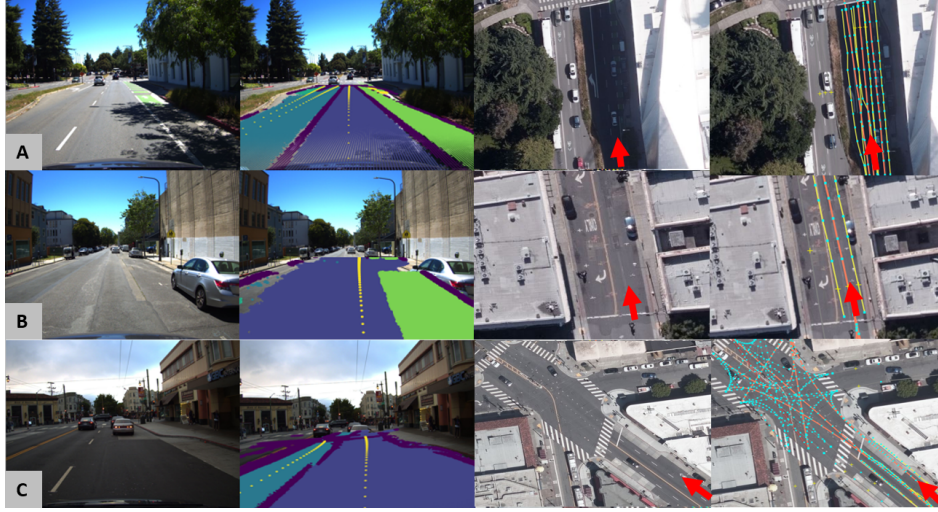


Fig.1 Roads in an urban environment are complicated: there are scenes with lane splitting (A), broken or no markings (B), and frequent irregularities like bus stops (C). Urban intersections are even worse: shown in C is a 6-way intersection in San Francisco. The proposed algorithm can explore the lane structure and intersection topology in such complex environments. The left two columns are camera inputs and generated HD maps overlapping the camera images: the aquamarine and blue areas represent left/center lanes; green represents other road elements like bike path or parking zones; and the purple and yellow dots are lane boundaries and reference trajectories for the ego vehicle. The right two columns are the satellite maps overlapped by the HD maps. Red arrows denote the corresponding ego vehicle pose.

Abstract—High definition (HD) maps have demonstrated their essential roles in enabling full autonomy, especially in complex urban scenarios. As a crucial layer of the HD map, lane-level maps are particularly useful: they contain geometrical and topological information for both lanes and intersections. However, large scale construction of HD maps is limited by tedious human labeling and high maintenance costs, especially for urban scenarios with complicated road structures and irregular markings. This paper proposes an approach based on semantic-particle filter to tackle the automatic lane-level mapping problem in urban scenes. The map skeleton is firstly structured as a directed cyclic graph from online mapping database OpenStreetMap. Our proposed method then performs semantic segmentation on 2D front-view images from ego vehicles and explores the lane semantics on a birds-eye-view domain with true topographical projection. Exploiting OpenStreetMap, we further infer lane topology and reference trajectory at intersections with the aforementioned lane semantics. The proposed algorithm has been tested in densely urbanized areas, and the results demonstrate accurate and robust reconstruction

of the lane-level HD map.

I. INTRODUCTION

High definition (HD) maps have become a crucial component for full autonomy in a variety of complex scenarios. Encoded with accurate and comprehensive information of the static environment, HD maps can significantly facilitate perception, localization, prediction and planing [1]. HD maps contain multiple layers of information abstractions, and the lane-level information plays the quintessential role in many applications. Embedded with lane geometries, road semantics, and connection topology, the lane layer can be utilized for defining potential region of interest (ROI) for some key modules in autonomous driving, including but not limited to object detection [2], regulating the lateral location of the ego vehicle [3], [4], and predicting behavior of other vehicles [5].

With numerous alluring applications, these lane-level HD maps, however, do not scale easily. Many of these HD maps are restricted to small scale environments due to the high costs in manual labeling and maintenance [6]. Recently, a few commercial products have been launched to automatically map highways [7], where the lanes are structured and the markings are clear. In urban scenes,

^{*}Both authors contributed equally to this work. Yuichi Takeda completed this work during his visit at UC Berkeley.

¹Mechanical Systems Control Lab, University of California, Berkeley, CA, USA, 94705

²Nissan Motor Co. Ltd., 1-1 Morinosatoaoyama, Atsugi, Kanagawa, 243-0123, Japan

Correspondence: yiyang.zhou@berkeley.edu

however, the roads are much more complicated. As shown in the first and third column in Fig. 1, urban roads may have complicated forking, potholes, broken markings or even no markings at all. Furthermore, a city road also carries irregularities such as parking zones, bus curbs, and bike lanes. Also, the topological relationship of urban lanes are much more intricate at complicated intersections. As a result, the automatic lane-level mapping in urban areas remains as an open and challenging problem.

It is worth to notice that the lane-level HD map construction problem is different from geometry tasks like lane detection or trajectory inference. HD map requires a semantic and topological understanding beyond the instance level, meaning that the map should contain logic connections with geometric information. As compared with simple lane boundary regression, HD map constructors further infer the merging/forking relationship between lanes; as compared with trajectory inference, HD maps further address the lane topological relationship.

Previous works have regarded lane detection and intersection trajectory generation as separate problems, and most of these works only target on the geometric understanding of the scenes. In this work, we study lanes and intersections jointly and provide topological understanding beyond simple geometric representations.

In this paper, we firstly define the HD map representation as a directed cyclic graph (DAG) for easy data storage and query. We then propose a method based on semantic-particle filter to automatically generate an urban lane-level HD map with a front view camera and an optional LIDAR sensor. The proposed method contains three major components: a semantic segmentation network for scene understanding, a sequential Monte Carlo lane tracing module over bird's-eye-view (BEV), and an intersection inference module with OpenStreetMap (OSM) [8]. The whole pipeline only requires one single execution per road direction for a complete reconstruction of the lane-level details including the lane boundaries, reference trajectories, lane splitting information, and road topology. Lastly, we represent our generated lane map in a differentiable format for downstream modules. We test the proposed method in densely urbanized areas such as San Francisco and Downtown Berkeley from the UrbanLoco dataset [9], and some exemplar mapping results can be seen in Fig 1. The experiment covers areas with lane merging/splitting, missing/broken lane markings, complicated intersections, and irregular road shapes such as bus curbs and parking areas. The results demonstrate an accurate and robust construction of the lane-level HD maps.

The major contributions of this paper are:

- Propose to combine semantic scene understanding with Monte-Carlo sequential exploration for accurate and robust HD map construction in urban scenes.
- Infer geometrical representation and topological relationships for both lanes and intersections.
- Exploit OSM as a coarse prior map, and construct a directed cyclic graph representation of the urban road structure.

- Test the proposed algorithm with public dataset collected from densely urbanized area and validated the robustness and accuracy.

II. RELATED WORKS

With the map-related research advancing in the past few years, there are a number of attempts for automatic lane-level map construction. We will start by introducing geometrical inference works for lanes and intersections. Later, we will introduce methods with topological understanding contributing to an HD map construction.

A. Lane detection: markings

Since the lanes are defined by markings painted on the road surface, a natural way for lane-level map construction initiated from the lane marking detection perspective. Nieto et al. used a step-row filter [10] for lane marking detection and applies Rao-Blackwellized Particle Filter for lane tracing [11]. In [12], Li et al. used Convolutional Neural Network and Recurrent Neural Network for lane marking detection on highways. More recently, Garnett et al. [13] and Guo et al. [14] further used the 3D-LaneNet framework not only to classify the lane in an image, but also to predict its location in 3D.

These approaches achieve high quality marking detection on highway or suburban roads where the shape of the roads is simple and can be approximated by a polynomial-like functions. However, it is hard to implement the aforementioned methods to urban scenarios with complicated road structures, broken/missing lane markings, and frequent road splits. Furthermore, the method mentioned in [13] and [14] only works for scenarios with mild changes in 3D slope, disregarding the abrupt changes in road topography.

B. Lane detection: drivable areas

Some other methods focus on drivable areas for lane detection. Meyer et al. designed a neural network for ego and neighboring lane detection [15]. Kunze et al. created a scene graph from semantic segmentation to generate a detailed scene representation of the drivable areas and all road signage [16]. On the other hand, Roddick et al. used a pyramid projection network to extract the drivable area as well as other vehicles [17]. Neither of these methods were extended to the HD mapping domain, allowing a third vehicle to make full use of the detection results.

C. Intersection lane inference

Understanding the intersection structure is an indispensable technique for autonomous driving and HD Map generation. Thus a number of studies have been conducted to extract invisible lanes and connecting topology at intersections.

Trajectories of other vehicles have been commonly used for intersection exploration. For example, in [18] [19], the authors used vehicle trajectories acquired from on-board sensor such as stereo camera or LIDAR. Later, Meyer et al. used simulated vehicle trajectories and employed a Markov chain Monte Carlo sampling to reconstruct the lane topology

and geometry at both real and simulated intersections [20], [21]. In [22], [23], the authors used collected GPS data loaded on fleet vehicles. These methods have the potential to estimate lane-level structure of intersection, but they are data-hungry, and the performance heavily relies on the quality of vehicle trajectories, which themselves are non-trivial to acquire.

More recently, directly predicting road connections at intersections from camera images became another popular direction for lane inference. The work from Nvidia [24] formulates the inference problem as classification and chose the best trajectories from a real trajectory pool with cross entropy loss. And Paz et al. [25] predicts the trajectory from a Gated Recurrent Unit on a BEV semantic map. However, both methods only focus on the ego vehicle lane and predicts only one trajectory as a reference for the ego vehicle, not considering all visible lanes at an intersection.

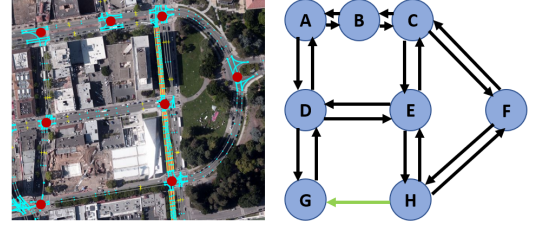
D. HD map generation

Large-scale map generation has long been considered as a Simultaneous Localization and Mapping (SLAM) problem [26]. However, instead of semantics, common SLAM algorithms focus more on the odometry estimation. Recently, in [6] and [27], the authors used semantics in the image domain and fuse semantic results with LIDARs to generate a semantic representation of the scene, not exactly an HD map. In terms of lane level map generation, a common approach is to accumulate extracted road environments along localization results [28], [29]. Both aforementioned approaches used LIDAR to extract road environments, and used OSM as a map prior. In [29], fork and merge of the lanes were able to be recognized by particle filter based lane marking tracking. Homayoundar et al. on the other hand, used a directed acyclic graph (DAG) and treated each detected lane marking as a node to decide future actions for connection, initiation, or termination [30]. However, these methods focused on road segments ignoring intersections, and they do not define the start and end point of the lanes. Thus, connections between lanes are not studied in these works. With the help of aerial images, authors of [31] studied both road sections and intersections. However, the method is limited by the availability and resolution of aerial images.

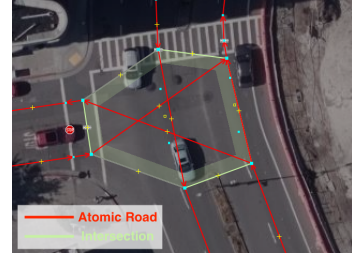
While the aforementioned efforts in lane detection and map generation has significant contributions to the community, they are limited to either simple road structures or single road segments. Our work targets specifically at the complicated urban driving scenes and considers both lane segments and intersection inference. Furthermore, we consider the topographical deformation of the road surface for more robust and accurate lane detection.

III. PRIMITIVE: MAP HIERARCHY

We depart from a topological point of view for this cartography task. A city road network is consisted of individual road segments and connecting intersections. As shown in Fig 2-a, an urban lane-level HD Map M could be further abstracted into a directional cyclic graph representation



(a) DAG Representation of the map M



(b) Intersection ROI

Fig. 2. Map hierarchy as a directed cyclic graph. Each intersection (red dot) in the satellite map is represented by a node I on the graph. The green edge E represents an one way road.

with each edge E_{ij} representing a directional road from an intersection node I_i to another intersection node I_j . We deliberately choose to have an edge for each direction due to the ubiquity of one-way roads and physically separated two-way roads in urban scenes (as shown in Fig 1. A). Previous works focused on either the edge E_{ij} or the node I_i for geometrical information extraction, but we study the HD map M containing both roads and intersections:

$$M := \{E_i, I_i\} \quad (1)$$

To acquire such a high-level map skeleton, we extract the coarse road-level topological information from OSM [8]. Disregarding the direction of travel for most roads, the OSM defines a road as a series of nodes connected together under a road instance. For special two-way roads with solid barrier as the median, OSM would have one road instance for each direction. Furthermore, the OSM defines an intersection as a connection node of two or more road instances. Although represented by a single node, the actual intersection is a geometrical region where multiple roads/lanes intersect. Utilizing such definition, we predict the intersection ROI (shown in Fig 2-b) with a polygon formed by the closest road node to the intersection node, leaving the rest of the road nodes as part of the atomic road.

With the atomic road E_{ij}^0 and intersection patch I_i^0 defined as the skeleton M^0 of our map, we are able to match the moving data collection vehicle to an atomic road or an intersection in the road network. Different from the goal variables M , E_{ij} and I_i , M^0 , E_{ij}^0 and I_i^0 contains neither geometric nor topological information of the lanes. Now we proceed to the proposed methodology for automatic map generation.

IV. METHOD

A. Problem formulation

To automatically generate the lane-level map from the aforementioned map skeleton M^0 , our proposed approach utilizes an on-board front-view camera C_t and an optional (represented by $*$) LIDAR L_t^* at time t . We also require the synchronized vehicle poses RT_t in the global coordinate, which come either from external sensors or SLAM algorithms. Representing our framework as a function $F(\cdot)$, the goal map shown in Equation 1 could be further described by:

$$M := \{E_i, I_i\} = F(C_t, L_t^*, RT_t, M^0) \quad (2)$$

The goal for atomic roads E_{ij} estimation is to infer lane k 's center line $\{L_k\}_K$ and its left-right boundaries $\{B_{k,left}, B_{k,right}\}_K$, where K is the number of lanes in this atomic road. We deliberately go beyond a lane width as an asymmetrical representation of lane boundary due to irregularities in the drivable areas of a lane (examples are in Fig.1 B and C). Here, L_k could be represented either as a continuous trajectory function and as a collection of way points, while discrete points $B_{k,left}, B_{k,right}$ would form an enclosed drivable area of the lane. As shown in Fig. 3, we would start with semantic segmentation ($S(C_t)$) of the camera image, and then use particles to explore the lane over the BEV domain, which is accumulated from $S(C_t)$, L_t^* , and RT_t . To be more specific, we are looking for:

$$E_{ij} = \{L_k, B_{k,left}, B_{k,right}\}_K = G_1(S(C_t), L_t^*, RT_t) \quad (3)$$

The goal for intersection I_i estimation is to infer the topological relationship and geometrical reference trajectory between $E_{.i}$ and $E_{.l}$ as a Bezier curve $\mathbf{B}(E_{.i}^k, E_{.l}^l)$, where k and l denotes specific lanes in atomic roads. When two lanes are not topologically connected, the function output is set to be null. Here, we are utilizing the result in the previously defined E_{ij} and the skeleton map M^0 for lane tracing at the intersection. Again, we study:

$$I_i = \{\mathbf{B}(E_{.i}^k, E_{.l}^l)\}_{K \times L} = G_2(E_i, M^0) \quad (4)$$

As an outline for the following sections, function $S(\cdot)$ is introduced in Section IV-B, function $G_1(\cdot)$ is introduced in Section IV-C, and function $G_2(\cdot)$ introduced in Section IV-D.

In corresponding maps shown in the bottom of Fig. 3, we start with a coarse map skeleton M^0 , go through the road semantics E_{ij} and reference trajectory I_i generation, and end with a lane-level HD map M .

B. Semantic understanding of the scene

Drivable areas and lanes are defined by the road markings painted on road surfaces, and lane markings in the urban areas are more complicated: there are numerous lane splitting, frequent stop lines and broken/missing markings.

Therefore, instead of only extracting lane markings from camera images, we consider this problem as semantic segmentation and infer both drivable areas and lane markings from camera images. Built upon a DeepLab-v3+ [32] structure, we are particularly interested in ego lanes, 2 neighboring lanes on each side of the ego lane, dashed lines, solid lines, crosswalks, road curbs, and stop lines. As shown in Fig. 4, the input of the network is an image C_t , and we predict the aforementioned 10 classes. These semantic instances forms the foundation of our understanding of the current scene. Considering both lanes and lane markings is especially efficient for urban scenes as the lane markings might be missing, and some drivable areas may be confused with parking zones.

C. BEV accumulation and atomic road structure estimation

After the road semantics are extracted from the camera images, the segmented images ($S(C_t)$) are projected onto the ground plane in map coordinates. These projected BEV images are then accumulated together for a semantic representation of the atomic road. For the scope of this semantic mapping problem, we assume that the pose of the ego vehicle RT_t is given from auxiliary sensors like inertia-GPS navigation systems or SLAM algorithms like [26].

For the BEV projection, most previous works assume a flat ground as the road model. However, such estimation is over-simplified in city scenes. For urban areas, undulating road surfaces, either purposefully designed for drainage or accidentally caused by lack of maintenance, are common. Fig. 5-left shows that by simply assuming a flat surface of the road, the BEV projection could be distorted. We propose to optionally use a synchronized LIDAR scan L_t^* as the ground topography, and then project the image on to a topography mesh. To generate the ground mesh from sparse point clouds, we process the synchronized LIDAR point cloud through a Delaunay Triangulation with each point as a vertex on the mesh. After LIDAR correction, the BEV projection could be seen in Fig. 5-right, where the distorted cross-walk markings are rectified. To further demonstrate the improvement of using the true ground topography, we include an ablation study of the map quality with/without the LIDAR correction in Section V-C.

With a semantic atomic road map shown as the background of 6-a, we now study the possible vehicle trajectories in such scenarios. To tackle the complicated, mostly irregular, driving scenes, we propose to use a Monte Carlo exploration strategy: the particle filter. Each particle represents a moving vehicle of an average sedan size with three state parameters: the BEV location and the yaw angle: $\chi_{n,t} = [x, y, \phi]_{n,t}^T$. The details of this exploration strategy is shown in Algorithm 1. With the ego vehicle starting at one end of the atomic road with RT_0 , we generate a strip of N particles $\{\chi_{n,t=0}\}_N$ perpendicular to the driving direction in RT_0 . Each particle $\chi_{n,t}$ then proceeds along the driving direction in the atomic lane map shown in Fig. 6-a. Here, we are simulating the actual driving of the car with speed v_m and yaw-rate ω_m

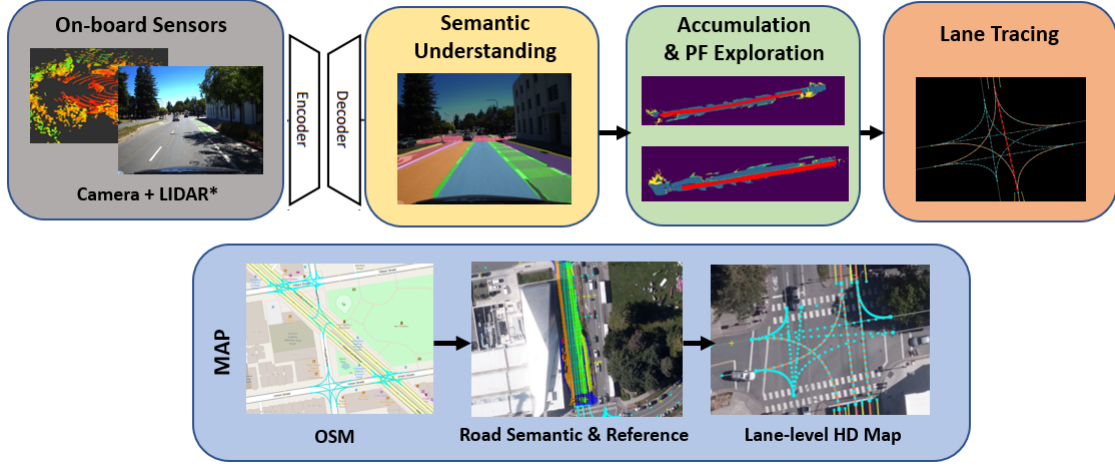


Fig. 3. The input of the proposed method is a series of camera images and LIDAR point clouds. We first process the camera image through a semantic segmentation module and then project the semantic instances onto the topographical mesh created by the LIDAR point cloud. We then accumulated the semantic projections from each frame to form a semantic map, in which a particle filter algorithm is carried out for lane regression. Lastly, we trace the lane connection at the intersection for topology.

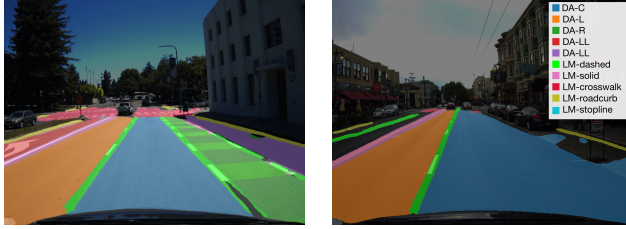


Fig. 4. Example results of semantic understanding module. This module extracts not only the lane marking but also the lane itself. DA- represents Drivable Area, which is Center, Left, Right, LeftLeft, RightRight respectively. LM- is a prefix of road marking class.

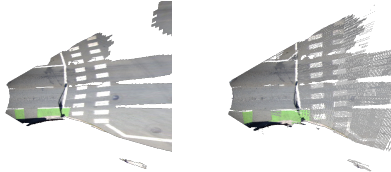


Fig. 5. BEV projection comparison with LIDAR (left) and without LIDAR (right). Without LIDAR, the crosswalk is significantly distorted.

uniformly sampled from noisy linear and angular velocity distribution V_m, Ω_m . The dynamic update function is

$$\overline{\chi_{n,t+1}} = \chi_{n,t} + \begin{bmatrix} \cos(\phi_{n,t} + \omega_m) * v_m \\ \sin(\phi_{n,t} + \omega_m) * v_m \\ \omega_m \end{bmatrix} \Delta t \quad (5)$$

Each predicted particle $\overline{\chi_{n,t+1}}$ will be re-weighted for its overlapping ratio with the lane boundaries (Fig. 6-b), and the weight is saved as $w_{n,t+1}$. Particle will be terminated at I_j . Through the sequential Monte Carlo process, we could simulate vehicle behaviors at lane splitting scenes. For unstructured roads too narrow to fit two lanes, particle filter also demonstrated a preferred driving trajectory of the vehicle

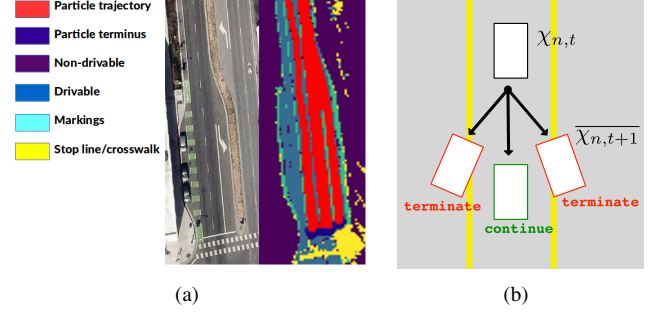


Fig. 6. (a): Particle history plotted next to the satellite map. The particles were exploring the forking at this atomic road. (b): Prediction and evaluation step of particle filter. Particle at time t ($\chi_{n,t}$) evolve by Eq. 5. Each predicted particle $\chi_{n,t+1}$ will be evaluated by BEV semantic map. If the particle overlaps with lane boundary, it will be terminated, and the only particles doesn't touch will continue to next step.

(Fig.1 B).

For particles travelled to the end of the atomic road $\{\chi_{n,T}\}$, we first clustered these particles with geometrical clustering algorithm DBSCAN [33] to determine the resulting number of lanes. Then we performed numerical regression to find the best representation of these lanes. After experimenting different regression models, we concluded that the best fit would be a optimized piece-wise linear regression smoothed with natural spline. By minimizing the sum-of-squared regression loss shown in Equation 6, we first determined the optimal break points b_i for the piece-wise regression function $f(x_n, b_i)$, and then used the natural spline to smooth the connection for a differentiable curve representation. Such differentiable form of reference trajectory is particularly valuable for further path-planning and prediction tasks [5].

$$L_k = f(x_n, \underset{b_i}{\operatorname{argmin}}(\sum_{t=0}^T \sum_{n=1}^N (y_n - f(x_n, b_i))^2)) \quad (6)$$

Sampling way points for each regressed lanes L_k , we

estimate the lane width by probing to the latitudinal direction of the lane. As a result, we would get accurate lane width $B_{k,left}, B_{k,right}$ at each specific sampled location. Together we form the atomic road map E_{ij} introduced in Equation 3 with reference trajectories L_k their lane boundaries $B_{k,left}, B_{k,right}$. It is worth to notice that such representation could be easily transferred to a LaneLet2 [34] format for further tasks.

Algorithm 1: Lane Exploration Particle Filter

Result: Returns the regressed lane on atomic roads on E_{ij}
initialize N particles $\{\chi_{n,t=0}\}_N$ with RT_0 and size;
while $\chi_{n,t}$ not at I_j **do**
 $\{\overline{\chi}_{n,t+1}\}_N, \{w_n\}_N = \emptyset$;
 for n in 1 to N **do**
 sample $\overline{\chi}_{n,t+1}$ from Equation 5 with V_n and Ω_n ;
 $w_n = \text{evaluate } \overline{\chi}_{n,t+1}$;
 $\{\overline{\chi}_{n,t+1}\}_N \leftarrow \overline{\chi}_{n,t+1}; \{w_n\}_N \leftarrow w_n$;
 end
 for n in $1:N$ **do**
 draw i from $\{w_n\}$;
 $\{\chi_{i,t+1}\} \leftarrow \chi_{i,t+1}$;
 save particle history;
 end
end
cluster $\{\chi_{n,T}\}$ in C with DBSCAN;
for c_k in C **do**
 $L_k = f(x_k, b_k | x_k \in c_k)$
 $B_{k,left}, B_{k,right} \leftarrow \text{Longitude explore } L_k$
end

D. Intersection lane tracing

As previously introduced in Equation 4, the road connection topology and reference trajectories inferences inside an intersection I_i come from the OSM skeleton M^0 and the lanes generated on neighboring atomic roads E_i and $E_{i'}$. Since the OSM defines the road connecting topology, we transfer this relationship to the lane level with general traffic rules: i.e. left lanes in E_i would connect to left lanes in $E_{i'}$; and the algorithm is demonstrated in Algorithm 2. Without explicit supervision, the topological inference would reach over 90% precision in urban areas. Based on the topology, reference trajectories are then regressed with a optimized second-order Bezier curve shown in Equation 7. We optimize Equation 7 for smoothness over the variable $\alpha \in [0, 1]$. The Bezier curve's head and tail correspond to the lane's location $L_{k_1,-1}$ and $L_{k_2,0}$ as shown in Fig. 7, and we used intersecting point of lines extending along the direction from the head and tail nodes as control point P for the curve.

$$\mathbf{B}(E_{ji}^{k_1}, E_{il}^{k_2}, \alpha) = (1 - \alpha)^2 L_{k_1,-1} + 2\alpha(1 - \alpha)\mathbf{P} + \alpha^2 L_{k_2,0} \quad (7)$$

Algorithm 2: Lane inference in intersection

Data: E_{ji}, E_{il} : set of incoming and outgoing atomic roads to intersection I_i^0
Result: returns set of lanes I_i for intersection I_i^0
connections = \emptyset
for E_{in} in E_{ji} **do**
 for E_{out} in E_{il}^0 **do**
 $N_{in} = \text{num_lanes}(E_{in})$
 $N_{out} = \text{num_lanes}(E_{out})$
 for k in 1 to $\min(N_{in}, N_{out})$ **do**
 connections = connections $\cup \{(E_{in}^k, E_{out}^k)\}$
 end
 end
end
 $I_i = \emptyset$
for $\{(E_{in}^k, E_{out}^k)\}$ in connections **do**
 $\mathbf{B}_k = \text{Bezier curve from Equation 7}$
 $I_i = I_i \cup \mathbf{B}_k$
end
return I_i

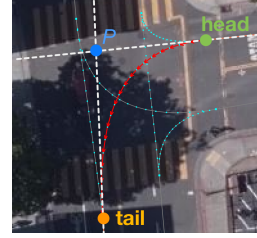


Fig. 7. Lane inference in intersection. We use second-order Bezier curve for lane geometry inference in intersection. The Bezier curve has 3 control points. Head and tail comes from last and first node of connected lanes, and the intermediate control point P is a intersecting point of lines extending the direction from head and tail nodes. The red line represents inferred lane center, and gray lines with blue dots are other lanes in this intersection.

V. EXPERIMENTS

A. Experimental Setup

To validate the proposed method, we have created lane-level HD maps for 3.5 KM routes in 47 blocks of the San Francisco Bay Area. The data is from a public mapping dataset [9] with front-view camera, LIDAR, and ground-truth ego-vehicle pose. To evaluate the atomic road and intersection reconstruction IOU, we manually label the drivable areas on Bing [35], and we performed a global rectification [36] for alignment as the maps and the ground truth were generated in different coordinate systems. To quantify the trajectory deviation, we use the trajectory from another driver passing through the same scenes on a different day.

For the semantic understanding module, We adopt DeepLab-v3+ [32]. We pre-train the module with the Cityscapes dataset [37] and fine-tuned with the BDD100K dataset [38]. Since BDD100K dataset only defines ego-lane and alter lanes for drivable areas, we extend this label to ego-lane, left lane, two left lane, right lane, and two right lanes. We use SDG as optimizer with learning rate 0.01,

TABLE I
ATOMIC ROAD MAPPING EVALUATION

Approaches	Location Name	Urbanization Rate	Sensor Input	Reported Results			
				RMS Error (m)	mIOU	Precision	Recall
Ours	Downtown Berkeley	Dense	LIDAR+Cam	0.24	0.79	0.84	0.73
			Cam	0.25	0.73	0.64	0.56
	San Francisco	Dense	LIDAR+Cam	0.33	0.76	0.63	0.63
Mattyus et al. [31]	Karlsruhe	Low	Aerial+Cam	0.57	0.55	0.86	0.60
Meyer et al. [15]	Frankfurt	High	Stereo	---	0.58	---	---
Paz et al. [6]	San Diego, CA	Medium	LIDAR+Cam	---	0.71	0.78	---
Joshi et al. [29]	King, MI	Low	LIDAR	0.06	---	---	---
Elhousni et al. [27]	Not Known	Medium	LIDAR+Cam	0.30	---	---	---

TABLE II
INTERSECTION INFERENCE EVALUATION

Approaches	Location Name	Urbanization Rate	Sensor Input	Evaluation Metrics		
				Precision	Recall	RMS Error (m)
Ours	Downtown Berkeley	Dense	LIDAR+Cam	0.91	0.80	0.24
		Dense	Cam	0.90	0.81	0.30
	San Francisco	Dense	LIDAR+Cam	0.93	0.90	0.46
Geiger et al [18]	Karlsruhe	Medium	Stereo	---	0.92	3.00
Joshi et al [19]	King, MI	Low	LIDAR	---	0.96	0.5
Meyer et al [20]	Karlsruhe	Low	Simulation	---	0.85	0.27
Roeth et al [22]	Not Known	Medium	Fleet DGPS	---	---	5.2

momentum 0.9, and batch size 4. Fine tuning is done for 250,000 steps. Images are resized to 512×512 on semantic segmentation process and restored to original size on BEV projection.

For BEV accumulation, we use the ground-truth localization provided in [9]. In the particle filter exploration, we deployed 500 particles, each with a length of 3m and a width of 1.5m. The velocity (m/s) is drawn uniformly from $U(0.9, 1.1)$, and the yaw angle (radian) is uniformly drawn from $U(-0.2, 0.2)$. The maximum cluster distance for DBSCAN is set to be 1m, which is around half of a typical lane with in urban scenes.

B. Lane-level map in Berkeley and San Francisco

A qualitative atomic road mapping result is shown in Fig. 1: the proposed method could successfully map lane-splitting (A), un-structured roads (B), and complicated intersections (D). For quantitative studies on lane-level HD maps, we do not find a consensus in academia for map quality evaluation. However, we use all popular metrics in previous works to demonstrate the effectiveness of our algorithm: the root-mean-square (RMS) error between the reference trajectory and ground truth, the mean intersection of union (mIOU) index of the proposed lane boundary, and the precision-recall values. All the evaluations are performed on per-lane basis. To study the detection rate of the proposed approach, we define a successful detection as one having over 0.7 mean IOU or less than 0.2m of RMS. A quantitative study of the proposed methods could be seen in Table 1.

Gauged at 0.7 mIOU or 0.2m RMS, our proposed methods has a mean RMS of 24cm for lane center trajectory estimation, and an average IOU of 0.79 for lane boundary estimation in Downtown Berkeley. With the same threshold, we are able to achieve 0.84 in precision and 0.73 in recall.

In North Beach, San Francisco, our approach has a RMS of 0.33m and mIOU of 0.76 when gauged at 0.7 IOU with 0.63 precision and 0.63 recall.

To the best of our knowledge, most previous endeavors in the similar filed use private data for evaluation, and we could not test our proposed approach on their dataset. More critically, most mapping-related algorithms and parameters are close-sourced, making it impossible to re-evaluate on our dataset. Thus, Table 1 lists the performance of other proposed methods [29], [27], [6], [31], [15] in similar matrices. We also list the urbanization rate at each location for a qualitative review of the difficulties for mapping at these areas.

For the invisible topology and trajectory inference in intersections, we evaluate our performance by the topological relationship precision-recall index as well as the inference trajectory RMS error. A quantitative results for the intersection could be seen in Table 2. Compared with a series of other methods in less urbanized areas, our algorithm is still able to discover the potential topological relationship at intersections with a lower RMS error.

C. Ablation study: true road topography

To study the effect of the road topography on our mapping system, we compare the map generated with true road topography and the map generated with a plane assumption of the ground. A quantitative comparison is shown in Table 1 and 2. It is clear that, with the LIDAR corrected topography, we have a significant improvement in atomic road detection precision and recall score. Also the estimated drivable area are closer to our labelled ground truth.

VI. CONCLUSION AND FUTURE WORKS

We have demonstrated that an HD map could be constructed automatically in complicated urban scenes with

a well-designed framework. Semantic understanding and Monte Carlo exploration strategy form the core of our proposed method. By employing particle filters on the accumulated semantic BEV maps, we are able to discover the atomic road structures. Furthermore, by exploiting OSM, we inferred both topological and geometrical connections at intersections. Tested in densely urbanized areas, our proposed approach enables large-scale HD map constructions, further facilitating downstream modules for full autonomy. In the current pipeline, semantic segmentation on 2D images limited our capacity at heavily occluded scenes. For next step, we plan to employ amodal prediction pipelines to directly predict semantic maps in the BEV domain.

REFERENCES

- [1] H. G. Seif and X. Hu, "Autonomous driving in the icity—hd maps as a key challenge of the automotive industry," *Engineering*, vol. 2, no. 2, pp. 159–162, 2016.
- [2] B. Yang, M. Liang, and R. Urtasun, "Hdnet: Exploiting hd maps for 3d object detection," in *CoRL*, 2018.
- [3] W.-C. Ma, I. Tartavull, I. A. Bârsan, S. Wang, M. Bai, G. Mattyus, N. Homayounfar, S. K. Lakshminathan, A. Pokrovsky, and R. Urtasun, "Exploiting sparse semantic hd maps for self-driving vehicle localization," 2019.
- [4] C. Tsuchiya, Y. Takeda, and A. Khiat, "A self-localization method for urban environments using vehicle-body-embedded off-the-shelf sensors," in *2019 IEEE Intelligent Vehicles Symposium (IV)*, pp. 1159–1165, 2019.
- [5] J. Gao, C. Sun, H. Zhao, Y. Shen, D. Anguelov, C. Li, and C. Schmid, "Vectornet: Encoding hd maps and agent dynamics from vectorized representation," in *Proceedings of the IEEE Conference on Computer Vision and Pattern Recognition (CVPR)*, 2020.
- [6] D. Paz, H. Zhang, Q. Li, H. Xiang, and H. Christensen, "Probabilistic semantic mapping for urban autonomous driving applications," in *IEEE/RSJ International Conference on Intelligent Robots and Systems (IROS)*, 2020.
- [7] Nvidia, "Nvidia drive mapping," 2020.
- [8] OpenStreetMap contributors, "Planet dump retrieved from <https://planet.osm.org>," <https://www.openstreetmap.org>, 2017.
- [9] W. Wen, Y. Zhou, G. Zhang, S. Fahandezh-Saadi, X. Bai, W. Zhan, M. Tomizuka, and L.-T. Hsu, "Urbanloco: A full sensor suite dataset for mapping and localization in urban scenes," in *IEEE International Conference on Robotics and Automation*, 2020.
- [10] M. Nieto, J. Arróspide, and L. Salgado, "Road environment modeling using robust perspective analysis and recursive bayesian segmentation," *Mach. Vis. Appl.*, vol. 22, pp. 927–945, 11 2011.
- [11] M. Nieto, A. Cortés, O. Otaegui, J. Arróspide, and L. Salgado, "Real-time lane tracking using rao-blackwellized particle filter," *J. Real-Time Image Process.*, vol. 11, p. 179–191, Jan. 2016.
- [12] J. Li, X. Mei, D. Prokhorov, and D. Tao, "Deep Neural Network for Structural Prediction and Lane Detection in Traffic Scene," *IEEE Transactions on Neural Networks and Learning Systems*, vol. 28, pp. 690–703, 3 2017.
- [13] N. Garnett, R. Cohen, T. Pe'er, R. Lahav, and D. Levi, "3D-LaneNet: End-to-End 3D Multiple Lane Detection," in *International Conference on Computer Vision (CVPR)*, 2019.
- [14] Y. Guo, G. Chen, P. Zhao, W. Zhang, J. Miao, J. Wang, and T. E. Choe, "Gen-lanenet: A generalized and scalable approach for 3d lane detection," in *European Conference on Computer Vision (ECCV)*, 2020.
- [15] A. Meyer, N. O. Salscheider, P. F. Orzechowski, and C. Stiller, "Deep Semantic Lane Segmentation for Mapless Driving," in *IEEE International Conference on Intelligent Robots and Systems*, pp. 869–875, Institute of Electrical and Electronics Engineers Inc., 12 2018.
- [16] L. Kunze, T. Bruls, D. Suleymanov, and P. Newman, "Reading between the Lanes: Road Layout Reconstruction from Partially Segmented Scenes," in *IEEE Conference on Intelligent Transportation Systems, Proceedings, ITSC*, vol. 2018–November, pp. 401–408, Institute of Electrical and Electronics Engineers Inc., 12 2018.
- [17] T. Roddick and R. Cipolla, "Predicting semantic map representations from images using pyramid occupancy networks," in *2020 IEEE/CVF Conference on Computer Vision and Pattern Recognition (CVPR)*, pp. 11135–11144, 2020.
- [18] A. Geiger, M. Lauer, C. Wojek, C. Stiller, and R. Urtasun, "3D traffic scene understanding from movable platforms," *IEEE Transactions on Pattern Analysis and Machine Intelligence*, vol. 36, no. 5, pp. 1012–1025, 2014.
- [19] A. Joshi and M. R. James, "Joint probabilistic modeling and inference of intersection structure," in *2014 17th IEEE International Conference on Intelligent Transportation Systems, ITSC 2014*, pp. 1072–1078, Institute of Electrical and Electronics Engineers Inc., 11 2014.
- [20] A. Meyer, J. Walter, M. Lauer, and C. Stiller, "Anytime lane-level intersection estimation based on trajectories of other traffic participants," in *2019 IEEE Intelligent Transportation Systems Conference (ITSC)*, pp. 3122–3129, 2019.
- [21] A. Meyer, J. Walter, and M. Lauer, "Fast lane-level intersection estimation using markov chain monte carlo sampling and b-spline refinement," in *IEEE Intelligent Vehicles Symposium (IV)*, 2020.
- [22] O. Roeth, D. Zaum, and C. Brenner, "Road network reconstruction using reversible jump MCMC simulated annealing based on vehicle trajectories from fleet measurements," in *IEEE Intelligent Vehicles Symposium, Proceedings*, vol. 2016–August, pp. 194–201, Institute of Electrical and Electronics Engineers Inc., 8 2016.
- [23] Y. Chen and J. Krumm, "Probabilistic modeling of traffic lanes from GPS traces," in *GIS: Proceedings of the ACM International Symposium on Advances in Geographic Information Systems*, (New York, New York, USA), pp. 81–88, ACM Press, 2010.
- [24] J. Philion and S. Fidler, "Lift, splat, shoot: Encoding images from arbitrary camera rigs by implicitly unprojecting to 3d," in *Proceedings of the European Conference on Computer Vision*, 2020.
- [25] D. Paz, H. Zhang, and H. I. Christensen, "Tridentnet: A conditional generative model for dynamic trajectory generation," 2021.
- [26] S. Yang, X. Zhu, X. Nian, L. Feng, X. Qu, and T. Mal, "A robust pose graph approach for city scale LiDAR mapping," in *IEEE International Conference on Intelligent Robots and Systems*, pp. 1175–1182, Institute of Electrical and Electronics Engineers Inc., 12 2018.
- [27] M. Elhousni, Y. Lyu, Z. Zhang, and X. Huang, "Automatic building and labeling of hd maps with deep learning," in *AAAI Conference on Artificial Intelligence*, 2020.
- [28] C. Guo, K. Kidono, J. Meguro, Y. Kojima, M. Ogawa, and T. Naito, "A low-cost solution for automatic lane-level map generation using conventional in-car sensors," *IEEE Transactions on Intelligent Transportation Systems*, vol. 17, pp. 2355–2366, 8 2016.
- [29] A. Joshi and M. R. James, "Generation of accurate lane-level maps from coarse prior maps and lidar," *IEEE Intelligent Transportation Systems Magazine*, vol. 7, no. 1, pp. 19–29, 2015.
- [30] N. Homayounfar, J. Liang, W.-C. Ma, J. Fan, X. Wu, and R. Urtasun, "Dagmapper: Learning to map by discovering lane topology," *2019 IEEE/CVF International Conference on Computer Vision (ICCV)*, pp. 2911–2920, 2019.
- [31] G. Mattyus, S. Wang, S. Fidler, and R. Urtasun, "Hd maps: Fine-grained road segmentation by parsing ground and aerial images," in *Proceedings of the IEEE Conference on Computer Vision and Pattern Recognition (CVPR)*, June 2016.
- [32] L. C. Chen, Y. Zhu, G. Papandreou, F. Schroff, and H. Adam, "Encoder-decoder with atrous separable convolution for semantic image segmentation," in *Lecture Notes in Computer Science (including subseries Lecture Notes in Artificial Intelligence and Lecture Notes in Bioinformatics)*, vol. 11211 LNCS, pp. 833–851, Springer Verlag, 2 2018.
- [33] M. Ester, H.-P. Kriegel, J. Sander, and X. Xu, "A density-based algorithm for discovering clusters in large spatial databases with noise," *KDD'96*, p. 226–231, AAAI Press, 1996.
- [34] F. Poggenhans, J.-H. Pauls, J. Janosovits, S. Orf, M. Naumann, F. Kuhnt, and M. Mayr, "Lanelet2: A high-definition map framework for the future of automated driving," in *Proc. IEEE Intell. Trans. Syst. Conf.*, (Hawaii, USA), November 2018.
- [35] Microsoft, "Microsoft bing map," 2020.
- [36] J. Sturm, N. Engelhard, F. Endres, W. Burgard, and D. Cremers, "A benchmark for the evaluation of rgb-d slam systems," in *Proc. of the International Conference on Intelligent Robot Systems (IROS)*, Oct. 2012.
- [37] M. Cordts, M. Omran, S. Ramos, T. Rehfeld, M. Enzweiler, R. Benenson, U. Franke, S. Roth, and B. Schiele, "The cityscapes dataset for

semantic urban scene understanding,” in *Proc. of the IEEE Conference on Computer Vision and Pattern Recognition (CVPR)*, 2016.

- [38] F. Yu, H. Chen, X. Wang, W. Xian, Y. Chen, F. Liu, V. Madhavan, and T. Darrell, “Bdd100k: A diverse driving dataset for heterogeneous multitask learning,” in *IEEE/CVF Conference on Computer Vision and Pattern Recognition (CVPR)*, June 2020.